THE *ASPERGILLUS FUMIGATUS* SIALIDASE IS A KDNASE: STRUCTURAL AND MECHANISTIC INSIGHTS

Judith C. Telford[*], Juliana H.F. Yeung[+], Guogang Xu[*], Milton J. Kiefel[‡], Andrew G. Watts†, Stefan Hader†, Jefferson Chan[¶], Andrew J. Bennet[¶], Margo M. Moore[+] and Garry L. Taylor[*]

From the [*]Biomedical Sciences Research Complex, University of St Andrews, St Andrews, Fife KY16 9ST, UK, and the [+]Department of Biological Sciences and [¶] Department of Chemistry, Simon Fraser University, 8888 University Drive, Burnaby, BC, Canada, V5A 1S6, the [‡]Institute for Glycomics, Griffith University, PMB 50 Gold Coast Mail Centre, Queensland 9726, Australia, and †Department of Pharmacy and Pharmacology, University of Bath, Bath, BA2 7AY, UK.

Running title: *Aspergilllus fumigatus* KDNase

Address correspondence to: Garry Taylor, Centre for Biomolecular Sciences, University of St Andrews, St Andrews, Fife KY16 9ST, UK, Tel. 44-1334-467301; Fax. 44-1334-462595; E-Mail: glt2@st-andrews.ac.uk.

***Aspergillus fumigatus* is a filamentous fungus that can cause severe respiratory disease in immunocompromised individuals. A putative sialidase from *A. fumigatus* was recently cloned and shown to be relatively poor in cleaving N-acetylneuraminic acid (Neu5Ac) in comparison to bacterial sialidases. Here we present the first crystal structure of a fungal sialidase. When the apo structure was compared to bacterial sialidase structures, the active site of the *Aspergillus* enzyme suggested that Neu5Ac would be a poor substrate due to a smaller pocket that normally accommodates the acetamido group of Neu5Ac in sialidases. A sialic acid with a hydroxyl in place of an acetamido group is 2-keto-3-deoxynononic acid (KDN). We show that KDN is the preferred substrate for the *A. fumigatus* sialidase and that *A. fumigatus* can utilise KDN as a sole carbon source. A 1.45Å resolution crystal structure of the enzyme in complex with KDN reveals KDN in the active site in a boat conformation, and nearby a second binding site occupied by KDN in a chair conformation, suggesting that polyKDN may be a natural substrate. The enzyme is not inhibited by the sialidase transition state analogue 2-deoxy-2,3-dehydro-N-acetylneuraminic acid (Neu5Ac2en) but is inhibited by the related KDN2en that we show bound to the enzyme in a 1.84Å resolution crystal structure. Using a fluorinated KDN substrate, we present a 1.5Å resolution structure of a covalently bound catalytic intermediate. The *A. fumigatus* sialidase is therefore a KDNase with a similar catalytic mechanism to Neu5Ac exosialidases, and this study represents the first structure of a KDNase.**

Sialic acids comprise the most chemically and structurally diverse carbohydrate family. Over 50 naturally occurring analogues exist, the majority based on 5-acetamido-3,5-dideoxy-D-*glycero*-D-*galacto*-non-2-ulosonic acid (*N*-acetylneuraminic acid, Neu5Ac, **1**) and 3-deoxy-D-*glycero*-D-*galacto*-non-2-ulosonic acid (2-keto-3- deoxynononic acid, KDN, **2**) that only differ at the C5 position (1). KDN, like Neu5Ac, occurs widely in bacteria and vertebrates, is found in almost all types of glycoconjugates including glycolipids, glycoproteins and capsular polysaccharides, and can be linked α2,3-, α2,4-, α2,6- or α2,8- to other carbohydrates (2). KDN was first discovered in the cortical alveolar polysialoglycoprotein of rainbow trout eggs as the capping carbohydrate on polysialic acid chains that were resistant to bacterial sialidases (3). In mammals, KDN was first identified in various tissues including human lung carcinoma cells but at a much lower abundances than Neu5Ac (4), and was subsequently found on human red blood cells and ovarian cancer cells (5). The development of linkage specific KDN antibodies (6,7) has allowed the identification of α2,8-linked polyKDN in many mammalian tissues (8), including the human lung (9).

Sialidases, or neuraminidases, catalyse the removal of terminal sialic acids from a variety of glycoconjugates and play an important role in pathogenesis, bacterial nutrition and cellular interactions. Crystal structures of a growing number of *exo*-sialidases that cleave Neu5Ac are available from bacteria (10-16), viruses (17-19), trypanosomes (20,21), leech (22) and man (23). All sialidases share the same six-bladed β-propeller fold for their catalytic domains, with conservation of key catalytic amino acids (24). The non-viral sialidases have an R-I/L-P motif containing one of the three active site arginines, and also have up to five

bacterial neuraminidase repeats (BNRs) or Asp-boxes (S/T-X-D-[X]-G-X-T-W/F). The BNRs occur at topologically identical positions in the β-propeller fold, remote from the active site, but any function beyond dictating a structural fold is unknown. Like many glycosyl hydrolases, sialidases can possess carbohydrate-binding modules (CBMs) in addition to the catalytic domain, placed upstream, downstream or even inserted within the β-propeller domain. It has been suggested that the presence of these CBMs increases the catalytic efficiency of the sialidases, particularly in the presence of polysaccharide substrates (25). In the case of sialidases having CBMs, these often recognise sialic acid as has been shown for the sialidases from *Vibrio cholerae* (26), *Clostridium perfringens* (27) and *Streptococcus pneumoniae* (15). Nearly all Neu5Ac-specific sialidases are inhibited by 2-deoxy-2,3-dehydro-*N*-acetyl-neuraminic acid (Neu5Ac2en, **3**), a putative transition-state analogue.

A sialidase specific for KDN ketosidic linkages was first discovered in the bacterium *Sphingobacterium multivorum*, and this so-called KDNase released KDN from naturally occurring substrates, including KDNα2-3Gal, KDNα2-6GalNAc, and KDNα2-8KDN linkages, but was not inhibited by Neu5Ac2en (28,29). The KDNase was however inhibited by 2,3-didehydro-2,3-dideoxy-D-*glycero*-D-*galacto*-nonulosonic acid (KDN2en, **4**) (30). Further analysis of this enzyme using synthetic KDN analogues suggested that the hydroxyl group at C5 was important for recognition of the inhibitor by the enzyme, and that like the Neu5Ac sialidases, the thermodynamically less stable α-form of the product is the first product of cleavage, suggesting a similar catalytic mechanism to the Neu5Ac exosialidases (30,31).

Aspergillus fumigatus is a common soil fungus and is the major species of *Aspergillus* that causes invasive aspergillosis in immunocompromised humans (32). Infection by *A. fumigatus* is mainly through inhalation of airborne conidiospores (conidia) that adhere to lung tissue. It has been shown that *A. fumigatus* conidia have surface sialic acids that may adhere to basal lamina proteins (33), and that pathogenic species of *Aspergillus* have a higher density compared to non-pathogenic species (34). The origin of these sialic acids remains a mystery, as although sialic acid biosynthesis has reported to occur *de novo* in *A. fumigatus* (34), its genome appears to lack the known Neu5Ac biosynthetic enzymes. In addition, *A. fumigatus* is incapable of utilising or incorporating exogenous Neu5Ac or ManNAc (35). Nevertheless, *A. fumigatus* does encode a sialidase that has recently been cloned and characterised (36).

The *A. fumigatus* sialidase has a 20-amino acid signal peptide, an RIP motif, one BNR, and shares 30% sequence identity with the bacterial sialidase from *Micromonospora viridifaciens* whose structure is known (37). The sequence of the *A. fumigatus* sialidase appears to possess the key active site residues of a sialidase: an arginine triad that interacts with the carboxylic acid group of sialic acids, a nucleophilic tyrosine (Tyr^{358}), its associated general acid (Glu^{249}), and an acid/base (Asp^{84}) (36).

In this study, we report the crystal structure of residues 21-406 of the *A. fumigatus* sialidase (herein after named *Af*S) determined by single wavelength anomalous diffraction from crystals of selenomethionine-derivitised protein. A comparison of the active site with the *M. viridifaciens* sialidase (*Mv*S) suggested that KDN might be a better substrate than Neu5Ac for the *A. fumigatus* enzyme, and we show kinetically that this is the case using the fluorescent substrate 4-methylumbelliferyl 3-deoxy-D-*glycero*-*α*-D-*galacto*-non-2-ulopyranosonic acid (KDN-MU, **6**). A 1.45Å resolution structure derived from a crystal of *Af*S soaked with KDN-MU revealed two KDN molecules bound to the enzyme: one in the active site and one in an adjacent position. *Af*S is not inhibited by Neu5Ac2en, but is inhibited by the KDN-related KDN2en (**4**), that we show bound in the active site of *Af*S in a 1.84Å resolution crystal structure. To complete a set of snapshots of the catalytic cycle, a 1.5Å resolution structure of a covalent intermediate was obtained with 2,3-difluoro-KDN (2,3F-KDN, **7**). NMR is used to show that catalysis of KDN-MU by *Af*S proceeds with retention of configuration at the anomeric carbon. Finally, we show that *A. fumigatus* can utilise KDN, and not Neu5Ac, as an effective sole carbon source. These studies suggest a nutritional role for *Af*S in the lifecycle of *A. fumigatus*, but also stimulate further studies into the potential role of KDN in the pathogenesis of the organism.

EXPERIMENTAL PROCEDURES

Expression and purification of AfS for structural studies- The *Af*S gene from the *A. fumigatus* clinical

isolate Af293 was amplified and ligated into the pET28A+ (EMD Chemicals Inc., San Diego, CA) vector and expressed in *Escherichia coli* (DE3) cells as previously described (36). Briefly, *E. coli* expressing the *Af*S/pET28A+ vector were grown in Luria Broth with 50 μg/ml kanamycin at 37 ℃, shaking at 220 rpm. Once the culture OD_{600} had reached 0.9 *Af*S expression was induced by 0.5 mM IPTG (Isopropyl thio-β-D-galactopyranoside) and incubated overnight. Cells were then harvested by centrifugation at 16,780g for 25 mins and re-suspended in phosphate buffered saline (50mM NaH_2PO_4, 300 mM NaCl, pH8) with EDTA-free Protease inhibitor cocktail (one tablet per 25 ml of solution; Roche Diagnostics) and DNase I (Sigma, final concentration 20 μg/ ml) and sonicated 5 times for 30 s. The sonicated culture was then centrifuged to remove insoluble cell debris at 37,000 g for 30 mins. The supernatant was then filtered through a 0.22 μm pore syringe driven filter before being loaded onto a 5ml HisTrap column (GE Healthcare) equilibrated with PBS. The bound protein was eluted with 5 column volumes of 300 mM imidazole in PBS. The eluted fraction was then subjected to size exclusion chromatography by loading onto a 120ml Sephacryl S-200 column (GE Healthcare). Fractions containing AfS were identified and purity assessed by SDS-PAGE and matrix-assisted laser desorption/ionisation time-of-flight mass spectrometry (MALDI-TOF MS). Fractions containing high purity *Af*S where then pooled, concentrated and diluted into 50 mM Tris-HCl, 100 mM NaCl, pH 8, then stored at -20 ℃.

Selenomethionine incorporation - *E. coli* expressing the *Af*S/pET28A+ vector were grown in 150 ml LB with 50 μg/ml at 37 °C, shaking at 220 rpm overnight. Cells were harvested by centrifugation at 16,800 g for 20 mins at 4 ℃. The supernatant was discarded and the pellet was re-suspended in 100 ml PBS and re-centrifuged. Supernatant was discarded and the pellet re-suspended in 4 ml PBS and added to 1 L sterile Selenomethionine (SeMet) media (17 mM NH_4Cl, 22 mM KH_2PO_4, 6 mM $Na_2HPO_4 \bullet 7H_2O$, 25 μM $Fe_2(SO_4)_3$ and 30 μM thiamine, 20% w/v glucose, 0.3% w/v $MgSO_4$). Addition of 50mg of selenomethionine and kanamycin (50μg/ml) was then made to the selenomethionine minimal media. The culture was incubated at 37 ℃ shaking at 200 rpm until OD_{600} reached 0.9 when *Af*S expression was induced by 0.5 mM IPTG and incubated overnight. Cells were harvested and *Af*S extracted and purified as above.

Protein crystallization - The optimal *Af*S concentration for crystal trials was determined as 13.7 mg/ml by pre-crystallization assay (Hampton Research). Sitting-drop vapour diffusion plates, held at 20 ℃ were used for all crystallization experiments. To ascertain crystallization conditions for *Af*S, commercial screens Cryo I and II (Emerald Biosystems), Crystal screens I and II and Index (Hampton Research), PEG screen (Qiagen) and Wizard (Emerald Biosystems) were used. Purified *Af*S was added to each screen condition in a 1:1 ratio by the high throughput Rhombix Screen robot. Crystals from the PEG screen (Qiagen), condition 20% (w/v) polyethylene glycol (PEG) 3350 and 0.2 M sodium nitrate, appeared after four days and did not require any optimisation. *Af*S with selenomethionine incorporated crystallised in identical conditions. The structures of *Af*S in complex with KDN, KDN2en and 2,3F-KDN were achieved by soaking *Af*S crystals by addition of 1 μl of 70 mM KDN-MU, 100 mM KDN2en (38) or 500mM 2,3F-KDN, respectively, to 4 μl well containing 1:1 ratio of 13.7 mg/ml *Af*S and 20% (w/v) PEG 3350 and 0.2 M sodium nitrate and leaving for 20 mins. The synthesis of KDN-MU and 2,3F-KDN is described in the supplementary information.

Data collection - Crystals were cryoprotected by transfer to 20% (w/v) glycerol in crystallization buffer for a few seconds prior to placement in liquid nitrogen. Native data and the KDN2en complex were collected at 100 K in-house (Rigaku-MSC Micromax-007 X-ray generator and Saturn 944+ CCD detector). Data at the selenium absorption edge, the KDN complex and the covalent complex were collected on beamlines ID23-1, ID29 and ID14-1, respectively, at the European Synchrotron Radiation Facility (ESRF), Grenoble. MOSFLM (39) and the CCP4 suite (40) were used to integrate and scale the diffraction data. Crystals of *Af*S belong to space group $P2_1$.

Structure determination and refinement - The structure of *Af*S was solved by SAD (single wavelength anomalous diffraction) using data collected at the selenium absorption peak. The selenium peak was at 0.9794Å , as determined by a crystal florescence scan. The selenium sites were determined using SHELXD (41) from the anomalous differences. SHELXE (41) was used to resolve the phase ambiguity and to apply density modification, resulting in an electron density map with a clear protein/solvent boundary and a polyalanine interpretation of the backbone of a large part of the structure. The phases from SHELXE

were used in Phenix (42), together with the amino acid sequence to automatically build an initial structure at 2.15Å. The model of the apo structure was refined in REFMAC5 (43) using in-house data collected from a SeMet crystal data to 1.84Å and manually fitted/improved with Coot (44) and validated by Coot and MolProbity (45). The structures of *Af*S in complex with ligands were refined similarly. Data collection and refinement statistics, together with PDB codes of the deposited structures are given in Table 1.

Sialidase and KDNase activity assays - The activity of enzyme preparations was determined by measuring cleavage of the synthetic sialic acid substrate, 4-methylumbelliferyl α-D-*N*-acetylneuraminide (Neu5Ac-MU, **5**, Sigma, Oakville, ON), or KDN-MU (synthesis described in supplementary materials). Briefly, reactions were set up in 96-well plates by adding 200 µM Neu5Ac-MU or KDN-MU, purified recombinant enzyme and the specific reaction buffer for a total volume of 100 µl. Plates were incubated at 37ºC for 10 minutes followed by the addition of 200 µl cold stop solution (0.1 M glycine, 0.014 M NaCl, 25% ethanol, pH 10.7). Following the addition of stop solution, the amount of 4-methylumbelliferone released from Neu5Ac-MU or KDN-MU was determined using a fluorescence spectrophotometer at excitation and emission wavelengths of 365 and 450 nm, respectively. Fluorescence produced during the course of the reaction was related to the concentration of Neu5Ac-MU or KDN-MU cleaved by comparison with a standard curve of 4-methylumbelliferone (Sigma). Each reaction was performed in triplicate.

Kinetic assay - Michaelis-Menten parameters for the *Af*S and *Mv*S were measured using Neu5Ac-MU or KDN-MU. Each 100µl reaction mixture was incubated at 37ºC for 1 minute prior to addition of either purified sialidase. The progress of the reaction was continuously monitored for 20 minutes using a fluorescence spectrophotometer equipped with a temperature controller set to 37ºC and excitation and emission wavelengths of 365 and 450 nm, respectively. For Neu5Ac-MU, kinetic parameters were determined from 19 initial rate measurements using a substrate concentration range of 50 µM to 5000 µM. For KDN-MU, kinetic parameters were determined from 22 initial rate measurements using a substrate concentration range of 10 µM to 800 µM. The rate versus substrate concentration data were fitted to the Michaelis-Menten equation using GraphPad (GraphPad Software Inc., San Diego, CA).

pH profile - The optimal pH of the purified enzyme was determined by measuring its specific activity (nmol. mg^{-1}. min^{-1}) towards KDN-MU in buffers of varying pH. The buffers used were 40 mM sodium formate (pH 3 - 3.5), 50 mM sodium acetate (pH 4 – 5), 16 mM sodium tartrate (pH 5.2), 32.5 mM 2-(N-morpholino)ethanesulfonic acid (MES) (pH 6 – 7), 40 mM 3-(N-morpholino)propanesulfonic acid (MOPS) (pH 6.5), and 50 mM Tris-HCl (pH 7.5 – 9). The ionic strength of all buffers was maintained at 100 mM with NaCl and all buffers were prepared for use at 37ºC.

Temperature profile - *A. fumigatus* sialidase activity towards Neu5Ac-MU or KDN-MU was measured in 40 mM sodium acetate at pH 4.0. The activity of the enzyme was evaluated at 10, 15, 20, 25, 30, 37, 40, 45, 50 and 60 °C. Each reaction mixture was incubated for 10 min and the amount of 4-MU released was determined as described above.

NMR experiments - ^{1}H NMR spectroscopy was used to examine product formation from the hydrolysis of KDN-MU by *Af*S and to test for *trans*-sialidase activity. Reaction mixtures included 15 µL 23 mg/ml *Af*S, 15 µL 33 mg/ml KDN in $^{2}H_2O$. In the case of the *trans*-sialidase assay, 15 µL 20 mg/ml galactose or N-acetylgalactosamine in $^{2}H_2O$ was also added. The reaction mixture was then made up to 600 µl with PBS pH 7 in $^{2}H_2O$ and placed in a 5 mm NMR tube. Reaction mixtures were incubated at room temperature and spectra recorded at 0, 0.5, 1, 5, 12 and 24 hours. All NMR spectra were recorded at 298 K using a 500 MHz Bruker spectrometer taking 64 scans with a 2 s relaxation delay. During the relaxation delay the remaining water signal was suppressed by continuous low power irradiation.

Carbon source utilization - To determine the preferred carbon source use by *A. fumigatus*, 10^4 *A. fumigatus* spores were inoculated per well in 96-well plates containing chemically defined media with 25 mM carbon source of glucose, mannose, KDN, or sialic acid, or with no carbon source. All carbon sources were tested in triplicate. The KDN contained a maximum of 5% mannose; therefore, a K(+0.05MAN) sample, which contains 1.25 mM mannose, was tested to ensure that the small amount of mannose in the KDN sample did not contribute significantly to fungal growth. All media were adjusted to ~ pH 6.5 prior to inoculation. A paraffin

overlay (50 µl) was added to each well to prevent cross contamination of spores between wells. All plates were placed in a moist chamber and incubated at 37°C. Growth of the fungus was monitored spectrophotometrically at OD 620nm (Expert Plus Microplate Reader, Biochrom Asys).

RESULTS

Overall structure - The structure of *Af*S was solved by SAD phasing. The asymmetric unit contains two *Af*S molecules that superimpose with an rmsd of 0.43Å , but do not form any significant association (buried surface area ~400Å ^{2}). The closest structural homologue to *Af*S is *Mv*S (PDB code 1eus) where 311 C_α atoms (chain A) or 309 C_α atoms (chain B) of *Af*S overlay *Mv*S with an rmsd of 1.52Å and 1.44Å , respectively. *Af*S has the canonical, six-bladed β-propeller fold of a sialidase with an excursion between strands 2 and 3 of the second propeller blade, involving residues 142-172, that forms a cap region above the active site (Figure 2). A more extensive excursion at the same topological position exists in the NanI sialidase from *Clostridium perfringens* (13) and the NanA/NanB sialidases from *Streptococcus pneumoniae* (15,16). *Af*s is a basic protein with a theoretical pI of 9.3, and this is reflected in the electrostatic potential surface that shows a predominantly positive surface around the active site and extending in a groove down and below the molecule (Figure 2). This is in contrast to secreted bacterial sialidases that tend to have a highly acidic surface on one side that, it is suggested, helps orient the enzyme in the neighbourhood of a negatively charged surface (13,15,26). Behind the active site and below the cap domain there is a metal binding site (Figure 2). The bond lengths are consistent with the binding of sodium or calcium. The metal ion is secured by the side chains of Asp^{87} and Asn^{89} as well as the backbone carbonyls of Gly^{116} and Gly^{118}. Two water molecules sit directly above and below the metal ion completing the octahedral stabilisation of the ion.

A superposition of the *Mv*S-Neu5Ac2en complex (PDB code 1eus) onto *Af*S shows conservation of key residues in the active site (Figure 3). These include the arginine triad, the nucleophilic tyrosine and its associated glutamic acid, and the acid/base aspartic acid. Neu5Ac2en is not an inhibitor of *Af*S, and this may be explained, in part, by the presence of Arg^{171} in *Af*S protruding into the hydrophobic pocket that usually accommodates the acetamido group of Neu5Ac2en (Figure 3). This suggested that *Af*S recognises a sialic acid with a smaller group at C5. The only sialic acids with a smaller group at C5 are neuraminic acid, that has an amino group at C5 but does not occur naturally, and KDN that has a hydroxyl at C5 (1).

Kinetic analysis shows AfS prefers KDN over Neu5Ac – Michaelis-Menten parameters for *Af*S were measured using Neu5Ac-MU or KDN-MU as substrates. *Af*S had a K_m of 5.8 ± 1.7 mM and a catalytic efficiency (k_{cat}/K_m) of 0.86 $M^{-1}s^{-1}$ for Neu5Ac-MU; however for KDN-MU it had a K_m of 0.23 ±0.02 mM and a catalytic efficiency of (1.82 ± 0.091) x10^5 $M^{-1}s^{-1}$. *Mv*S has a reported k_{cat}/K_m of (7.23 ± 0.04) x 10^6 $M^{-1}s^{-1}$ (47), therefore *Af*S has a similar catalytic efficiency with KDN-MU as *Mv*S has with Neu5Ac-MU. AfS has a pH optimum of between 3.5 and 4.5 with KDN-MU, similar to its optimum with Neu5Ac-MU (36). The optimal temperature range of *Af*S with KDN-MU was from 30 to 37 °C.

Crystal structure of AfS complexed with KDN – The structure derived from a crystal of *AfS* soaked in KDN-MU revealed two αKDN molecules bound per monomer (Figures 4, 5). One KDN occupies the active site and is in a boat conformation, the second occupies a positively-charged site (site 2 in Figure 2) adjacent to the active site such that the distance from the anomeric oxygen of the active site KDN is only 6.4Å from C9 and 7.7Å from C8 of the second KDN. Intriguingly, in monomer B, there is a glycerol molecule from the cryoprotectant sitting between the two KDN molecules (Figures 4,5).

Active site of AfS – KDN in the active site is bound in its α-anomeric form, with the ring adopting a distorted $B_{2,5}$ boat conformation. The O2 hydroxyl of KDN forms a close interaction (2.57Å) with Asp^{84} and also interacts with the bound glycerol (2.71Å). Although there are a number of significant differences between the active sites of viral, bacterial and eukaryotic sialidases, a number of key features have been retained throughout their evolution (24), and are shown in Figure 4. These include a tri-arginal cluster (Arg^{59}, Arg^{265}, Arg^{322}) that interacts with the carboxylate group of KDN. The position of the first arginine (Arg^{59}) is stabilised by a conserved glutamic acid (Glu^{374}). A tyrosine (Tyr^{358}) and a glutamic acid (Glu^{249}) hydrogen bond with each other and sit beneath and close to the C1-C2 bond of the substrate. A conserved feature of sialidase active sites is the acid/base catalyst, Asp^{84}. The O7 and O9 hydroxyls of the KDN glycerol group interact with Gln^{148} that extends down from

the cap region, and the O8 hydroxyl interacts with Glu^{249}. The O4 of KDN interacts directly with Arg^{78} and also makes several water-mediated interactions with the enzyme. All active sites of sialidases that hydrolyse Neu5Ac have a hydrophobic pocket to accommodate the N-acetyl group of the substrate at C5, but the exact residues that form this pocket are generally not conserved. In *Af*S, although the pocket around the C5 hydroxyl of KDN has two hydrophobic residues lining it, Trp^{202} and Ala^{204}, the pocket is predominantly polar and filled with water molecules. O5 of KDN does not make direct contact with *Af*S, but interacts with Asn^{124} and Glu^{249} via a water molecule, and with Asn^{142}, Glu^{56} and Trp^{202}, via two water molecules. At its closest approach, Arg^{171} is only ~4.5Å from O5 of KDN. If the structure of the *C. perfringens* NanI sialidase in complex with $B_{2,5}$ αNeu5Ac (PDB code 2bf6) is superimposed on AfS, then the acetamido methyl group of Neu5Ac would be <2.5Å from Arg^{171}. Therefore, Arg^{171} appears to be a major determinant of *Af*S being a KDNase. Arg^{171} packs on one side of the indole ring of Trp^{202}, with Gln^{148} packing on the other side, and together may define a KDN-recognition sequence motif.

Second KDN binding site – KDN in the second site is also in its α-anomeric form, with the ring adopting a $^2C_5$ chair conformation. This KDN is possibly a bound KDN-MU, although no electron density is visible for the methylumbelliferyl moiety. This KDN makes only 4 direct hydrogen bonds with *Af*S: O4 makes two interactions with the guanidinium group of Arg^{323}, O1B interacts with the backbone amide of Arg^{322}, and O5 interacts with Asp^{376}. In addition, multiple water-mediated interactions are made involving all the oxygens of KDN apart from O8 and O9. The ring of KDN sits in a cavity sandwiched ~4.5Å above the methylene groups of Arg^{322} and ~4.0Å below Phe^{378} (Figures 4 and 5). It is unlikely that this second site could bind Neu5Ac as the pocket around O5 is polar and in particular the presence of Arg^{388} would preclude the binding of the acetamido group of Neu5Ac. This hypothesis is supported by repeated failed attempts to visualize Neu5Ac in either KDN binding site in the crystal.

KDN2en complex - The 1.84Å resolution structure shows that KDN2en adopts a $^4H_5$ half-chair conformation. The distance between the hydroxyl of Tyr^{358} and C2 of the ligand shortens to 2.81Å, compared to 3.23Å in the KDN complex. All interactions with *Af*S, both direct and water-mediated are identical in the two complexes (Figure 6).

Covalent intermediate – The 1.5Å resolution structure clearly shows 3-fluoro-β-KDN (3F-β-KDN) covalently linked to Tyr^{358} in an unstrained $^2C_5$ conformation (Figure 7A) as observed in the *T. cruzi trans*-sialidase (48), *T. rangeli* sialidase (49) and *C. perfringens* NanI (13) covalent complexes. The covalent bond refines to a length of 1.75Å. The presence of the fluorine at C3, and its close proximity (2.7Å) to the acid/base Asp^{84}, appears to lead to a dual conformation being observed for the side chain of this residue, something that was observed in the NanI complex. The second binding site observed in the KDN complex is here occupied by 2,3F-KDN in the same $^2C_5$ chair conformation. Additionally, there are three more 2,3F-KDN molecules bound in the asymmetric unit in a $^2C_5$ conformation. Two are at the same site on each monomer of *Af*S (site 3 in Figure 2), and the third sits at the interface between the monomers (site 4 in Figure 2). The O4 hydroxyl of 2,3F-KDN in site 3 interacts with the sidechain of Ser^{330}, and backbone atoms of Lys^{337} and Tyr^{331}, while O5 interacts with the sidechain of Asp^{332}.

NMR monitoring of KDN-MU hydration by AfS – (Figure 8) The hydrolysis of KDN-MU to form KDN was monitored as a time course reaction using ^{1}H NMR spectroscopy in deuterated buffer at a pD of 3.6. The $H3_{eq}$ proton of KDN-MU has a characteristic doublet of doublets (δ = 2.75 ppm, $J_{3e,3a}$ = 12.7 Hz, $J_{3e,4}$ = 4.7 Hz). With the addition of *Af*S, cleavage of the umbelliferyl group leads to a shift of the $H3_{eq}$ resonance to δ = 2.60 ppm of the αKDN product. Over time αKDN mutarotates to the thermodynamically more stable βKDN with the appearance of $H3_{eq}$ resonance at δ = 2.10 ppm. No *trans*-sialidase activity was observed for *Af*S (data not shown).

A. fumigatus can utilise KDN as a sole carbon source – To determine whether KDN could be a carbon source for *A. fumigatus*, we measured growth in defined media supplemented with various carbon sources (Figure 9). The data indicate that *A. fumigatus* is unable to use Neu5Ac as the sole source of carbon; however, it is able to use KDN though less efficiently on a molar basis compared to glucose. There was also a short lag in growth suggesting that KDN catabolic enzymes must be induced prior to utilization of this substrate.

DISCUSSION

The structure of the sialidase (*Af*S) from *A. fumigatus* presented here represents the first structure of a fungal sialidase, and the first structure of a KDN-specific sialidase, or KDNase. The KDN complex reveals two KDN molecules bound per monomer (Figures 4&5). The structural details of this complex, the complex of *Af*S with KDN2en, and the covalent intermediate suggest a similar mechanism for *Af*S as has been described for other Neu5Ac-specific exo-sialidases, as all of the key catalytic residues are conserved and occupy near identical positions (Figure 3). Although the αKDN in the active site is the product of KDN-MU hydrolysis, it has its sugar ring in a strained and distorted $B_{2,5}$ conformation that is reminiscent of the induced sialic acid ring conformation seen in the Michaelis complexes between an aspartic acid mutant of *T.cruzi trans*-sialidase and α(2,3)-sialyl-lactose (48) and in wild-type NanI sialidase from *C. perfringens* with αNeu5Ac (13). This conformation of the sugar ring results in a pseudo-axial orientation of the glycosidic bond being cleaved, bringing it within 2.6 Å of the acid catalyst Asp^{84} for proton transfer. The supposed transition state, mimicked by the complex of *Af*S with KDN2en, changes the sugar ring to a half-chair $^4H_5$ conformation, reducing the distance between C2 and the hydroxyl of the nucleophile Tyr^{358} from 3.23Å to 2.81Å. The formation of the covalent bond in the intermediate captured with the fluorinated KDN substrate further shortens this distance to 1.75Å. In common with other sialidases, the active site is very rigid and only the hydroxyl of the Tyr^{358} sidechain moves by a maximum ~0.5Å (Figure 7B). With a KDN glycan it is likely that catalysis would proceed with the concomitant release of the aglycon moiety as described for other sialidases (13). This similarity between the mechanism of *Af*S and other sialidases is further supported by the NMR data (Figure 8) that show that catalysis proceeds with retention of configuration at the anomeric carbon of KDN.

The catalytic efficiency of *Af*S in cleaving the 4-methylumbelliferyl leaving group from KDN-MU is 10^5 times greater than its ability to cleave the same leaving group from Neu5Ac-MU. In addition, *Af*S is not inhibited by Neu5Ac2en, the transition state analogue of Neu5Ac-hydrolysing sialidases. The specificity of *Af*S KDNase for KDN lies in the nature of the pocket that accommodates the C5 hydroxyl, as had been predicted (30). Neu5Ac specific sialidases have a hydrophobic pocket to accommodate the acetamido group at C5; in contrast, *Af*S has a water-filled, polar pocket where modelling shows that Arg^{171} would clash with acetamido group of Neu5Ac. The hydroxyl at C5 of KDN does not interact directly with *Af*S, but makes several water-mediated interactions. Arg^{171}, the second arginine of an EGRR motif, sits one side of Trp^{202}, part of a WD motif, on the other side of which is Gln^{148} that interacts with the O7 and O9 hydroxyls of KDN. Do these three residues define a KDN-recognition motif? Extending a BLASTP search of the protein database with *Af*S (36), shows this **Q**-[~24aa]-EGR**R**-[~30aa]-**W**D motif to be conserved in the fungi *Neosartorya fischeri, A. terreus, Arthroderma gypseum, Trichophyton verrucosum, Microsporum canis, Chaetomium globosum* and *Nectria haematococca*, all of which share at least 72% sequence identity with *Af*S. A degenerate form of this motif, DGR**R**-[~30aa]-**W**, occurs in proteins annotated as sialidases from *Streptomyces bingchenggensis* and *Streptomyces avermitilis*. Arg^{171} in *Af*S sits at the start of the third strand of the second β-sheet of the β-propeller, and is seven residues before the start of an Asp-box. In the structures of Neu5Ac-sialidases, the equivalent residue occupying the same structural position is a serine (*C. perfringens, S. pneumoniae*), threonine (human Neu2) or leucine (*M. viridifaciens*), and the residue forms part of the larger, more hydrophobic pocket accommodating the acetamido group of Neu5Ac. Mutagenesis of Arg^{171} will perhaps show if this is a determinant of KDN binding.

The discovery of a second KDN binding site adjacent to the active site is an unusual finding for an exo-sialidase. Many bacterial and parasite sialidases or *trans*-sialidases possess additional carbohydrate-binding modules (CBMs) that often recognise sialic acid (15,26,27). The presence of these modules increases catalytic efficiency of the enzyme by targeting the sialidase to appropriate substrates (50). However, these CBMs are distinct domains and the sialic acid binding site in the CBM is typically at least 30 Å from the active site. In addition, bacterial sialidases often have an asymmetric charge distribution over their surface with the side opposite the active site being highly negatively charged, and this is thought to assist the orientation of the active site towards negatively-charged sialic acid substrates. In contrast, the surface of *Af*S is mainly positively charged and the

second KDN sits in a basic pocket only 7Å from the active site KDN. The second KDN is its α-anomeric form, with the ring adopting a low energy $^2C_5$ chair conformation, and with its anomeric oxygen pointing away from the surface of *Af*S. There is a positively charged groove running down and underneath the *Af*S surface beyond this second KDN (Figure 2). In the complex with a fluorinated KDN, two 2,3F-KDN molecules in a $^2C_5$ chair conformation occupy part of this groove. This is therefore suggestive of polyKDN being a preferred substrate of *Af*S. A positively-charged groove also extends along the surface of the bacteriophage K1F tailspike protein, an endosialidase that recognises and degrades α2,8-linked polyNeu5Ac (51).

We have shown that the *Af*S sialidase is a KDNase and may have a preference for polyKDN substrates. Why does *A. fumigatus* have a KDNase, and where in its lifecycle would it encounter KDN or polyKDN? We have shown that *A. fumigatus* can utilise KDN but not Neu5Ac as a sole carbon source, and this suggests a nutritional role for the KDNase in scavenging KDN from the environment. The few reports on the occurrence of KDN in bacteria show KDN to be part of the capsules and cell envelopes of pathogenic bacteria (reviewed in (2)). KDN was found to be a non-terminal part of complex surface oligosaccharides in *Klebsiella ozaenae* serotype K4, *Sinorhizobium fredii* strain SVQ293 and *Streptomyces sp*. MB-8. A polyKDN polymer, with the KDN molecules linked β2-4 to each other, was reported in the cell wall of the plant pathogen *Streptomyces sp*. VKM Ac-2124. Although there is little evidence to date, it may be possible that *A. fumigatus* finds sources of KDN in its natural ecological niche in soil where it survives and grows on organic debris.

A. fumigatus is the most prevalent airborne fungal pathogen, causing severe and often fatal invasive infections in immunocompromised hosts (reviewed in (32)). The conidia released by the fungus are small enough to reach the lung alveoli, and the resulting disease called invasive aspergillosis occurs predominantly in the lungs. Intriguingly, polyKDN has been found in the human lung, as well as in other tissues, identified through the use of a monoclonal antibody recognising α2,8-linked KDN molecules (4,9). PolyKDN in the lung is a relatively minor component of glycoproteins and glycolipids compared to Neu5Ac, and is reported to be associated with a developmentally-regulated 150kDa glycoprotein not present in adults, but present in various types of human lung tumours (52). The results presented here from a structural analysis of the *A. fumigatus* KDNase suggest further explorations into its role in nutrition or pathogenesis.

REFERENCES

1. Varki, A., and Schauer, R. (2009) Sialic Acids. in *Essentials of Glycobiology* (Varki, A., Cummings, R., Esko, J., Freeze, H., Stanley, P., Bertozzi, C., Hart, G., and Etzler, M. eds.), CSH Press. pp
2. Inoue, S., and Kitajima, K. (2006) *Glycoconj J* **23**, 277-290
3. Nadano, D., Iwasaki, M., Endo, S., Kitajima, K., Inoue, S., and Inoue, Y. (1986) *J Biol Chem* **261**, 11550-11557
4. Inoue, S., Kitajima, K., and Inoue, Y. (1996) *J Biol Chem* **271**, 24341-24344
5. Inoue, S., Lin, S. L., Chang, T., Wu, S. H., Yao, C. W., Chu, T. Y., Troy, F. A., 2nd, and Inoue, Y. (1998) *J Biol Chem* **273**, 27199-27204
6. Song, Y., Kitajima, K., and Inoue, Y. (1993) *Glycobiology* **3**, 31-36
7. Kanamori, A., Inoue, S., Xulei, Z., Zuber, C., Roth, J., Kitajima, K., Ye, J., Troy, F. A., 2nd, and Inoue, Y. (1994) *Histochemistry* **101**, 333-340
8. Ziak, M., Qu, B., Zuo, X., Zuber, C., Kanamori, A., Kitajima, K., Inoue, S., Inoue, Y., and Roth, J. (1996) *Proc Natl Acad Sci U S A* **93**, 2759-2763
9. Qu, B., Ziak, M., Zuber, C., and Roth, J. (1996) *Proc Natl Acad Sci U S A* **93**, 8995-8998
10. Crennell, S. J., Garman, E. F., Laver, W. G., Vimr, E. R., and Taylor, G. L. (1993) *Proc Natl Acad Sci U S A* **90**, 9852-9856
11. Crennell, S. J., Garman, E., Laver, G., Vimr, E. R., and Taylor, G. (1994) *Structure (Camb)* **2**, 535-544
12. Gaskell, A., Crennell, S. J., and Taylor, G. (1995) *Structure (Camb)* **3**, 1197-1205
13. Newstead, S. L., Potter, J. A., Wilson, J. C., Xu, G., Chien, C. H., Watts, A. G., Withers, S. G., and Taylor, G. L. (2008) *J Biol Chem* **283**, 9080-9088
14. Xu, G., Ryan, C., Kiefel, M. J., Wilson, J. C., and Taylor, G. L. (2009) *J Mol Biol* **386**, 828-840
15. Xu, G., Potter, J. A., Russell, R. J., Oggioni, M. R., Andrew, P. W., and Taylor, G. L. (2008) *J Mol Biol* **384**, 436-449
16. Xu, G., Li, X., Andrew, P. W., and Taylor, G. L. (2008) *Acta Crystallogr Sect F Struct Biol Cryst Commun* **64**, 772-775
17. Varghese, J. N., Laver, W. G., and Colman, P. M. (1983) *Nature* **303**, 35-40
18. Burmeister, W. P., Henrissat, B., Bosso, C., Cusack, C., and Ruigrok, R. W. H. (1993) *Structure (Camb)* **1**, 19-26
19. Crennell, S. J., Takimoto, T., Portner, A., and Taylor, G. (2000) *Nat Struct Biol* **7**, 1068-1074
20. Buschiazzo, A., Tavares, G. A., Campetella, O., Spinelli, S., Cremona, M. L., Paris, G., Amaya, M. F., Frasch, A. C., and Alzari, P. M. (2000) *Embo J* **19**, 16-24
21. Buschiazzo, A., Amaya, M. F., Cremona, M. L., Frasch, A. C., and Alzari, P. M. (2002) *Molecular Cell* **10**, 757-768
22. Lou, Y., Li, S.-C., Chou, M.-Y., Li, Y.-T., and Lou, M. (1998) *Structure (Camb)* **6**, 521-530
23. Chavas, L. M., Tringali, C., Fusi, P., Venerando, B., Tettamanti, G., Kato, R., Monti, E., and Wakatsuki, S. (2004) *J Biol Chem* **280**, 469-475
24. Taylor, G. (1996) *Curr Opin Struct Biol* **6**, 830-837
25. Thobhani, S., Ember, B., siriwardena, A., and Boons, G.-j. (2002) *J. AM. CHEM. SOC.* **125**, 7154-7155
26. Moustafa, I., Connaris, H., Taylor, M., Zaitsev, V., Wilson, J. C., Kiefel, M. J., von Itzstein, M., and Taylor, G. (2004) *J Biol Chem* **279**, 40819-40826
27. Boraston, A. B., Ficko-Blean, E., and Healey, M. (2007) *Biochemistry* **46**, 11352-11360
28. Kitajima, K., Kuroyanagi, H., Inoue, S., Ye, J., Troy, F. A., and Inoue, Y. (1994) *J Biol Chem* **269**, 21415-21419
29. Nishino, S., Kuroyanagi, H., Terada, T., Inoue, S., Inoue, Y., Troy, F. A., and Kitajima, K. (1996) *J Biol Chem* **271**, 2909-2913
30. Terada, T., Kitajima, K., Inoue, S., Wilson, J. C., Norton, A. K., Kong, D. C., Thomson, R. J., von Itzstein, M., and Inoue, Y. (1997) *J Biol Chem* **272**, 5452-5456
31. Terada, T., Kitajima, K., Inoue, S., Koppert, K., Brossmer, R., and Inoue, Y. (1996) *European journal of biochemistry / FEBS* **236**, 852-855
32. Latge, J. P. (1999) *Clin Microbiol Rev* **12**, 310-350

33. Wasylnka, J. A., and Moore, M. M. (2000) *Infect Immun* **68**, 3377-3384
34. Wasylnka, J. A., Simmer, M. I., and Moore, M. M. (2001) *Microbiology* **147**, 869-877
35. Tiralongo, J., Wohlschlager, T., Tiralongo, E., and Kiefel, M. J. (2009) *Microbiology* **155**, 3100-3109
36. Warwas, M. L., Yeung, J. H., Indurugalla, D., Mooers, A. O., Bennet, A. J., and Moore, M. M. (2010) *Glycoconj J* **27**, 533-548
37. Gaskell, A., Crennell, S., and Taylor, G. (1995) *Structure* **3**, 1197-1205
38. Sun, X.-L., Sato, N., Kai, T., and Furuhata, K. (2000) *Carbohydr Res* **323**, 1-6
39. Leslie, A. G. (2006) *Acta Crystallogr D Biol Crystallogr* **62**, 48-57
40. Bailey, S. (1994) *Acta Crystallographica Section D-Biological Crystallography* **50**, 760-763
41. Sheldrick, G. M. (2008) *Acta Crystallogr A* **64**, 112-122
42. Adams, P. D., Grosse-Kunstleve, R. W., Hung, L. W., Ioerger, T. R., McCoy, A. J., Moriarty, N. W., Read, R. J., Sacchettini, J. C., Sauter, N. K., and Terwilliger, T. C. (2002) *Acta Crystallographica Section D-Biological Crystallography* **58**, 1948-1954
43. Murshudov, G. N., Vagin, A. A., and Dodson, E. J. (1997) *Acta Crystallographica Section D-Biological Crystallography* **53**, 240-255
44. Emsley, P., and Cowtan, K. (2004) *Acta Crystallographica Section D-Biological Crystallography* **60**, 2126-2132
45. Lovell, S. C., Davis, I. W., Adrendall, W. B., de Bakker, P. I. W., Word, J. M., Prisant, M. G., Richardson, J. S., and Richardson, D. C. (2003) *Proteins-Structure Function and Genetics* **50**, 437-450
46. Potier, M., Mameli, L., Belisle, M., Dallaire, L., and Melancon, S. B. (1979) *Anal Biochem* **94**, 287-296
47. Watson, J. N., Dookhun, V., Borgford, T. J., and Bennet, A. J. (2003) *Biochemistry* **42**, 12682-12690
48. Amaya, M. F., Watts, A. G., Damager, I., Wehenkel, A., Nguyen, T., Buschiazzo, A., Paris, G., Frasch, A. C., Withers, S. G., and Alzari, P. M. (2004) *Structure* **12**, 775-784
49. Watts, A. G., Oppezzo, P., Withers, S. G., Alzari, P. M., and Buschiazzo, A. (2006) *J Biol Chem* **281**, 4149-4155
50. Thobhani, S., Ember, B., Siriwardena, A., and Boons, G. J. (2003) *Journal of the American Chemical Society* **125**, 7154-7155
51. Schulz, E. C., Schwarzer, D., Frank, M., Stummeyer, K., Muhlenhoff, M., Dickmanns, A., Gerardy-Schahn, R., and Ficner, R. *J Mol Biol* **397**, 341-351
52. Qu, B., Ziak, M., Zuber, C., and Roth, J. (1996) *Proc Natl Acad Sci USA* **93**, 8995-8998
53. Baker, N., Sept, D., Joseph, S., Holst, M., and McCammon, J. (2001) *Proc. Natl. Acad. Sci.* **98**, 10037-10041
54. The PyMOL Molecular Graphics System, Version 1.3, Schrödinger, LLC.

FOOTNOTES

JCT was supported by the Biotechnology and Biological Sciences Research Council (BBSRC). The resources of the Scottish Structural Proteomics Facility at St Andrews, funded by BBSRC, The Wellcome Trust and the Scottish Funding Council, were used for this project (GLT). MJK was the recipient of a Queensland International Fellowship. MMM and AJB are supported by the Natural Sciences and Engineering Research Council of Canada. Staff at the ESRF synchrotron and Dr Magnus Alphey are thanked for their assistance in X-ray data collection.

The abbreviations used are: Neu5Ac, 5-acetamido-3,5-dideoxy-D-*glycero*-D-*galacto*-non-2-ulosonic acid or *N*-acetylneuraminic acid ; Neu5Ac2en, 2-deoxy-2,3-dehydro-N-acetylneuraminic acid; Neu5Ac-MU, 4-methylumbelliferyl α-D-*N*-acetylneuraminic acid KDN, 3-deoxy-D-*glycero*-D-*galacto*-non-2-ulosonic acid or 2-keto-3- deoxynononic acid; KDN2en, 2,3-didehydro-2,3-dideoxy-D-*glycero*-D-*galacto*-nonulosonic acid; KDN-MU, 4-methylumbelliferyl 3-deoxy-D-glycero- α-D-galacto-non-2-ulopyranosonic acid.

TABLES

Table 1. Data collection and refinement statistics. Numbers in parentheses refer to the highest resolution shell.

$R_{merge} = \sum_{hkl} \sum_i |I_{hkl,\,i} - \langle I_{hkl} \rangle| / \sum_{hkl} \langle I_{hkl} \rangle$ *R-factor and R-free* $= (\Sigma \, | \, |F_o| - |F_c| \, |)/(\Sigma \, |F_o|)$

	SeMet 2.15	SeMet 1.84	KDN complex	KDN2en complex	Covalent intermediate
Data collection					
X-ray source	ID23-1	In house	ID29	In house	ID14-1
X-ray wavelength (Å)	0.9794	1.542	0.979	1.542	0.934
Resolution (Å)	58.2-2.15 (2.26-2.15)	12.4-1.84 (1.94-1.84)	37.3-1.45 (1.53-1.45)	12.4-1.84 (1.94-1.84)	31.1-1.50 (1.54-1.50)
Unit cell dimensions					
a(Å)	76.1	75.9	75.8	75.8	75.6
b(A)	58.2	58.2	58.0	58.1	58.1
c (Å)	94.7	94.7	94.8	94.4	94.4
β (°)		100.0	100.1	99.92	100.0
No. observations	318,537	228,526	504,295	214,982	342,750
Redundancy	7.1 (6.9)	3.1 (3.0)	3.5 (3.4)	3.1 (2.8)	3.1 (2.8)
Completeness (%)	99.9 (99.7)	84.2 (64.8)	99.5 (97.6)	98.8 (95.0)	86.2 (47.0)
R_{merge}	0.099 (0.137)	0.03 (0.196)	0.081 (0.245)	0.086 (0.153)	0.056 (0.29)
I/σI	14.6 (10.2)	15.6 (64.8)	9.4 (4.3)	9.8 (5.3)	12.9 (3.5)
Refinement					
Reflections used		61,943	142,319	69,250	111,035
N. atoms		7,000	7,287	7,129	7,265
Number of protein atoms		5,940	6,021	5,935	6,000
Number of water molecules		1,055	1,159	1,146	1,095
Number of ligand atoms		N/A	72	34	133
Average B-factor ($Å^2$)		11.8	12.2	9.1	13.9
Protein		9.5	9.5	7.0	11.3
Water		23.2	25.7	20.3	27.5
Ligand		N/A	18.7	8.4	18.2
R-factor	0.17	0.155	0.180	0.204	0.181
R-free	0.208	0.194	0.205	0.262	0.214
rmsd bond lengths (Å)	0.009	0.009	0.009	0.011	0.009
rmsd bond angles (°)	1.16	1.13	1.29	1.32	1.26
wwPDB code		2xcy	2xzi	2xzj	2xzk

FIGURE LEGENDS

Fig. 1. Chemical structures of ligands used in this study.

Fig. 2. Overall structure of *Af*S. Top: cartoon drawing drawn from blue at the N-terminus to red at the C-terminus. The black sphere below the cap domain and above the active site is a metal binding site. Bottom: a surface representation in the same orientations as the images above, colored according to electrostatic potential from -7KT to +7KT, calculated using APBS (53). This and other figures were drawn using PyMol (54). The locations of KDN binding sites observed in the crystal structures are indicated.

Fig. 3. Comparison of the active sites of *Af*S and *Mv*S. Stereo image showing a superposition of apo-*Af*S (green carbons) with a Neu5Ac2en complex of *Mv*S (grey carbons) (PDB code 1eus). Key conserved residues are labelled in the order *Af*s/*Mv*S, and Arg^{171} of *Af*S is highlighted.

Fig. 4. KDN recognition by *Af*S. (*A*) Stereo image of a Fo-Fc electron density map, contoured at 3σ. (*B*) Stereo image of the KDN binding sites showing hydrogen bond interactions (≤3.2Å) drawn as dotted lines.

Fig. 5. KDN bound in the active site (left) and second binding site, with the bound glycerol also shown.

Fig. 6. Complex of *Af*S with KDN2en. Stereo image of a Fo-Fc electron density map contoured at 2.5σ around KDN2en. Direct hydrogen bond interactions between the ligand and protein are shown.

Fig. 7. Covalent intermediate. (A) Stereo drawing showing the 2Fo-Fc electron density map (contoured at1σ) displayed around the 3-F-β-KDN covalently bound to Tyr^{358}. (B) Superposition of the complexes of *Af*S with KDN (green carbons), KDN2en (yellow carbons) and 3-F-β-KDN (magenta carbons). All protein carbon atoms are drawn in grey. The conserved interactions between the arginine triad and the carboxylate of the ligands are drawn as dotted lines.

Fig. 8. The ^{1}H NMR spectrum showing hydration of KDN-MU by *Af*S. The bottom spectrum is that of KDN-MU, and the upper spectra are taken at the time intervals shown after the addition of *Af*S.

Fig. 9. Growth of *A. fumigatus* on different carbon sources. K indicates the defined medium (Kafer's) with the additional carbon sources where Glu = glucose, Man = mannose, SA = Neu5Ac. All carbon sources were 25mM except for K (+0.05MAN) that contained 1.25 mM mannose.

Figure 1.

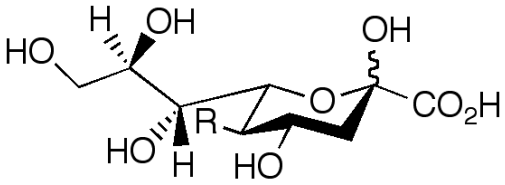

1 R = NHAc (Neu5Ac)
2 R = OH (KDN)

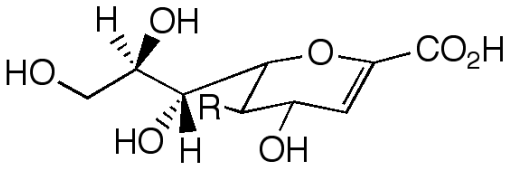

3 R = NHAc (Neu5Ac2en)
4 R = OH (KDN2en)

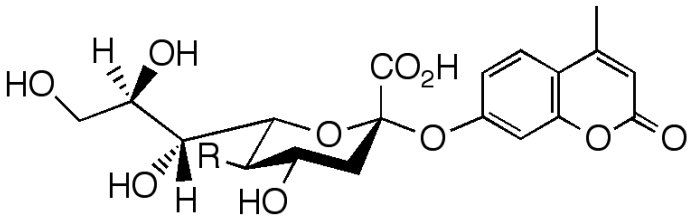

5 R = NHAc (Neu5Ac-MU)
6 R = OH (KDN-MU)

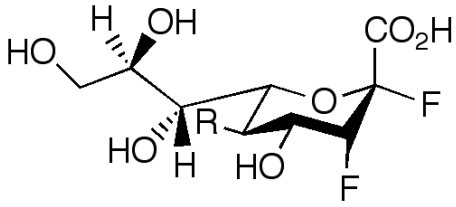

7 R = OH (2,3F-KDN)

Figure 2.

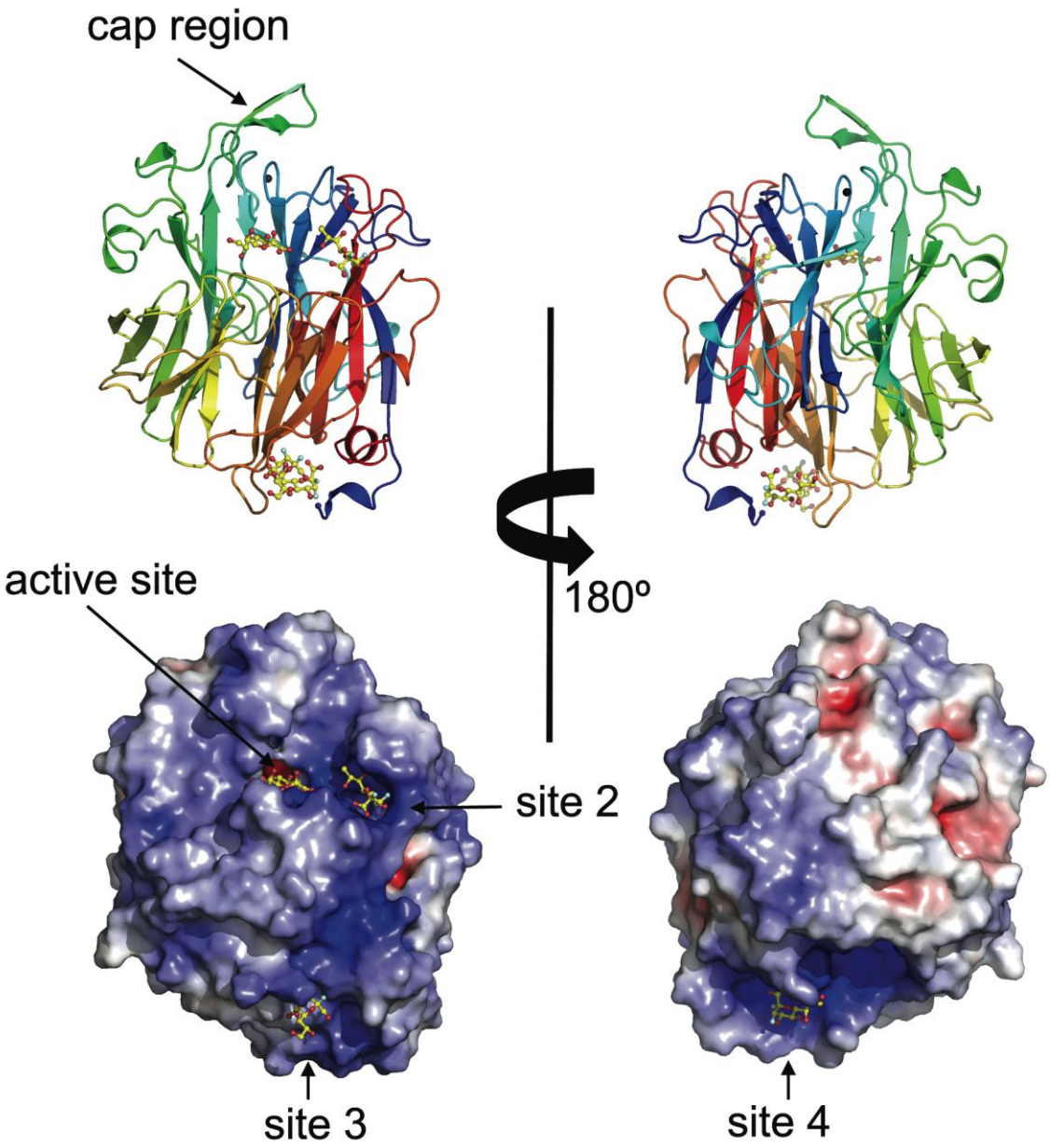

Figure 3.

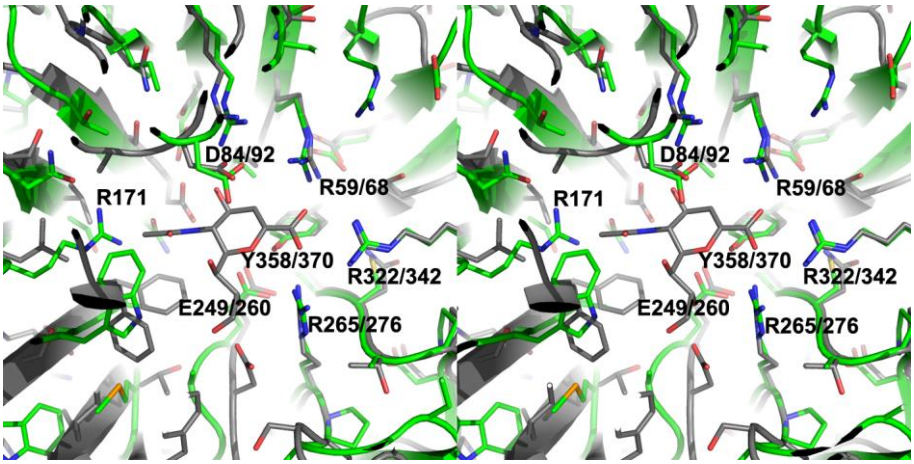
D84/92
R59/68
R171
Y358/370
R322/342
E249/260
R265/276
D84/92
R59/68
R171
Y358/370
R322/342
E249/260
R265/276

Figure 4.

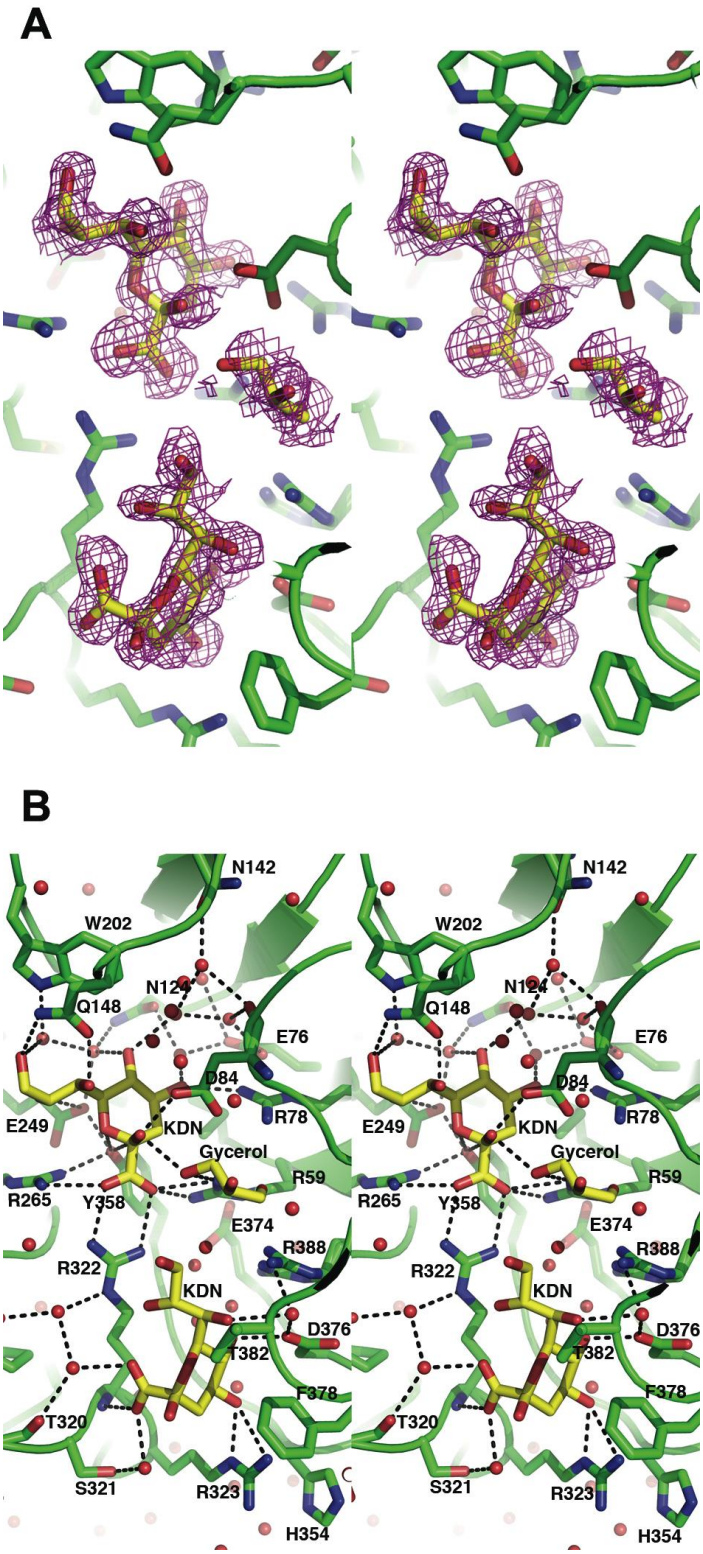
A
B
N142
W202
N124
Q148
E76
D84
R78
E249
KDN
Gycerol
R59
R265
Y358
E374
R388
R322
KDN
D376
T382
F378
T320
S321
R323
H354

Figure 5.

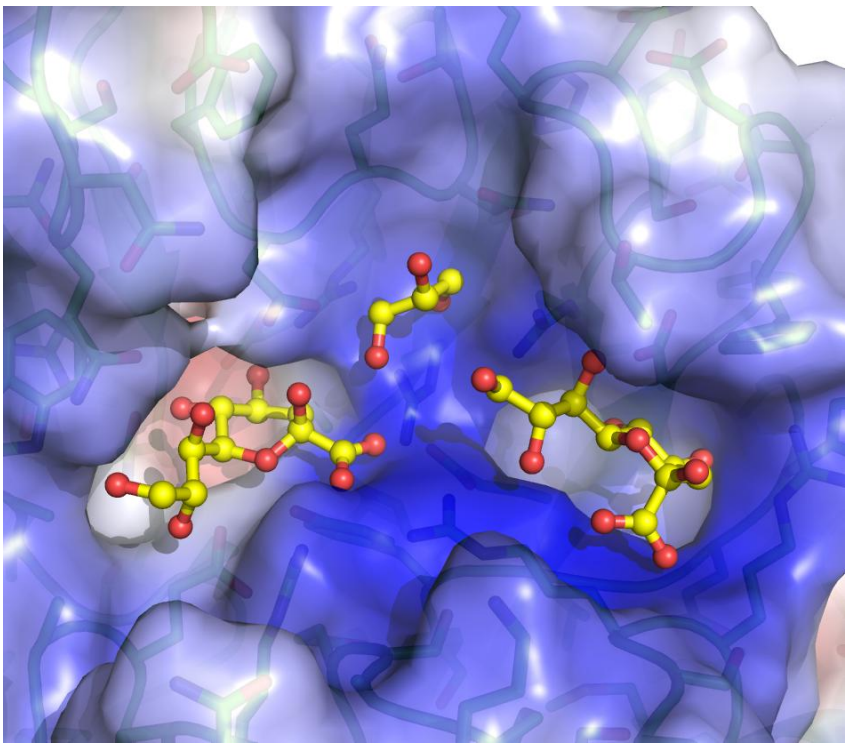

Figure 6.

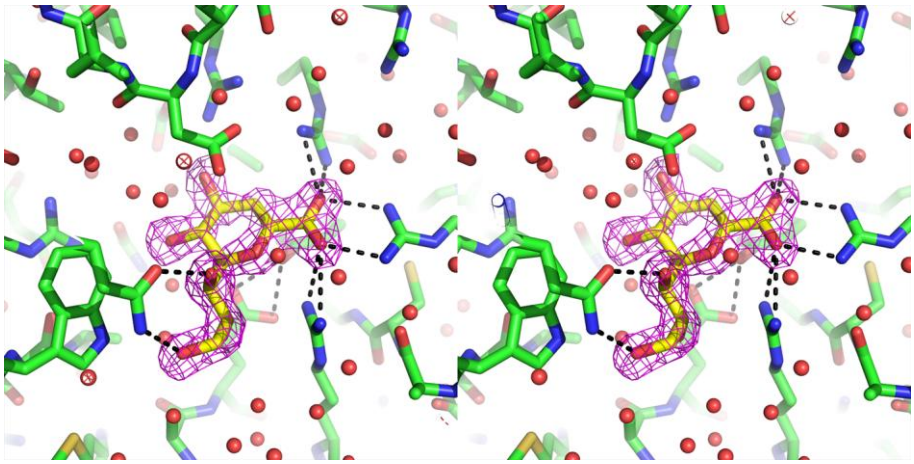

Figure 7

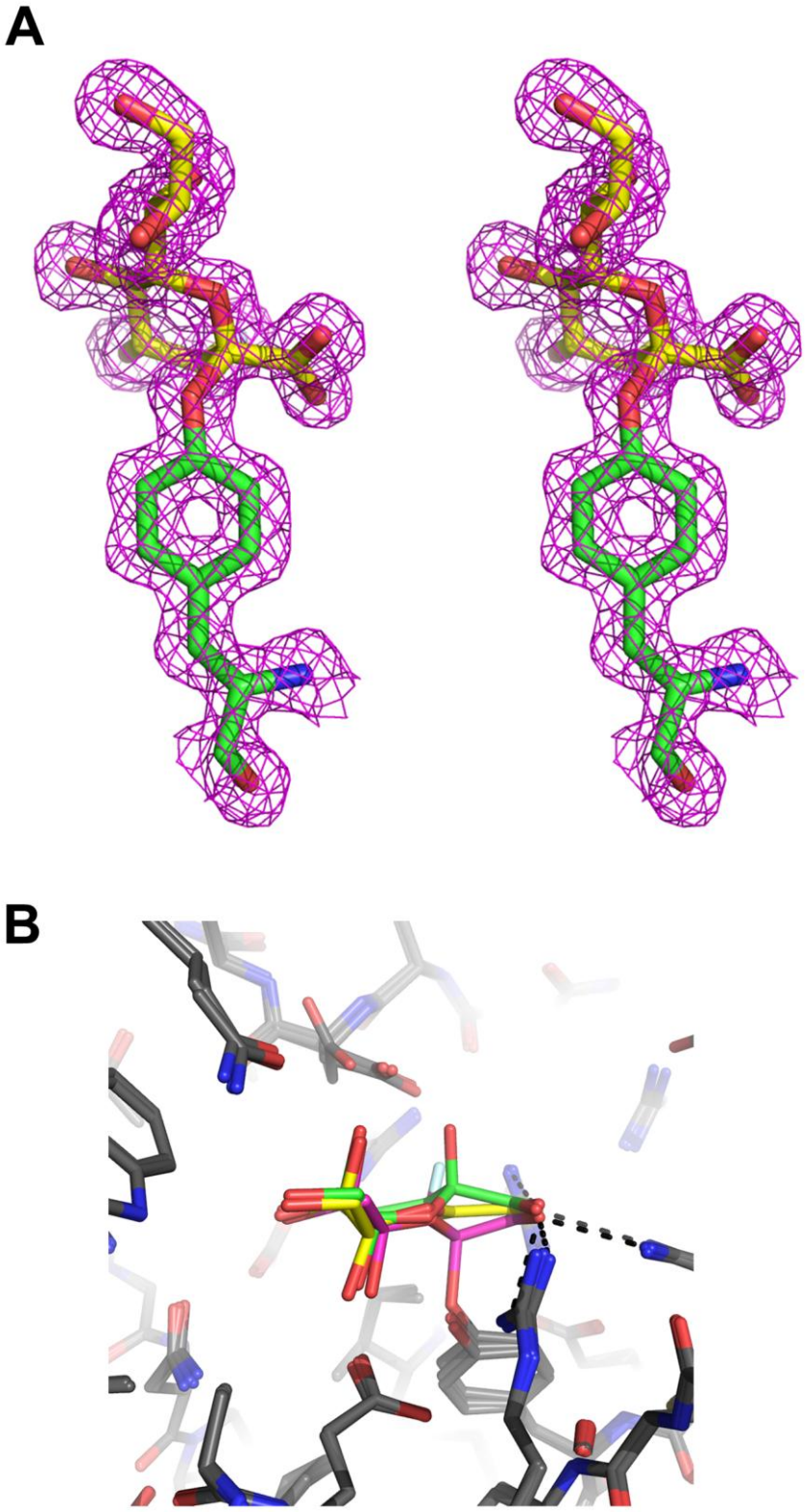

Figure 8.

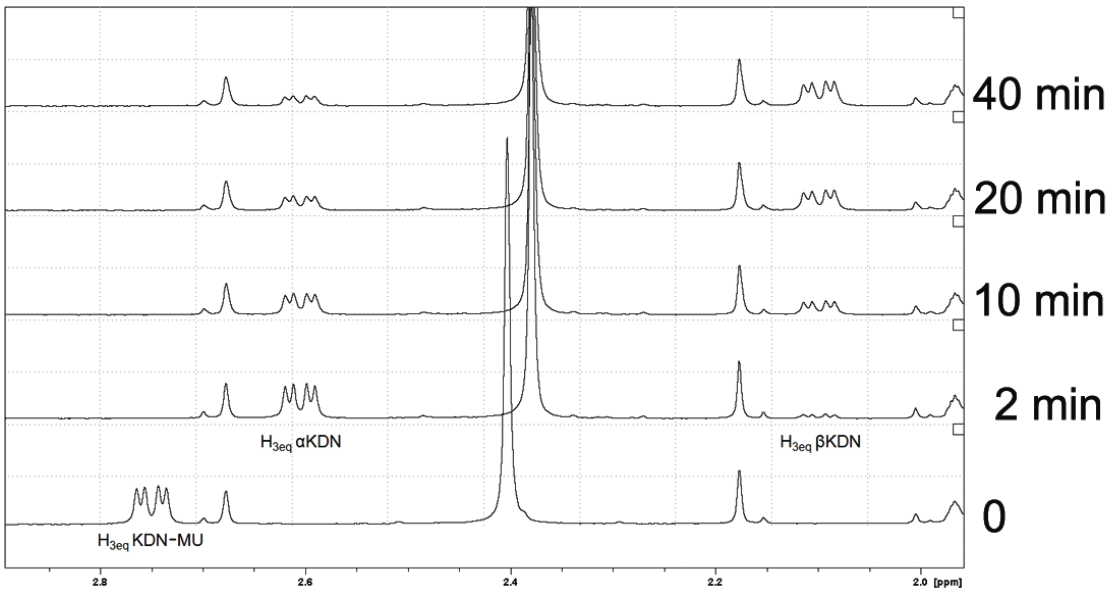
40 min
20 min
10 min
2 min
0
H3eq αKDN
H3eq βKDN
H3eq KDN-MU
2.8
2.6
2.4
2.2
2.0 [ppm]

Figure 9.

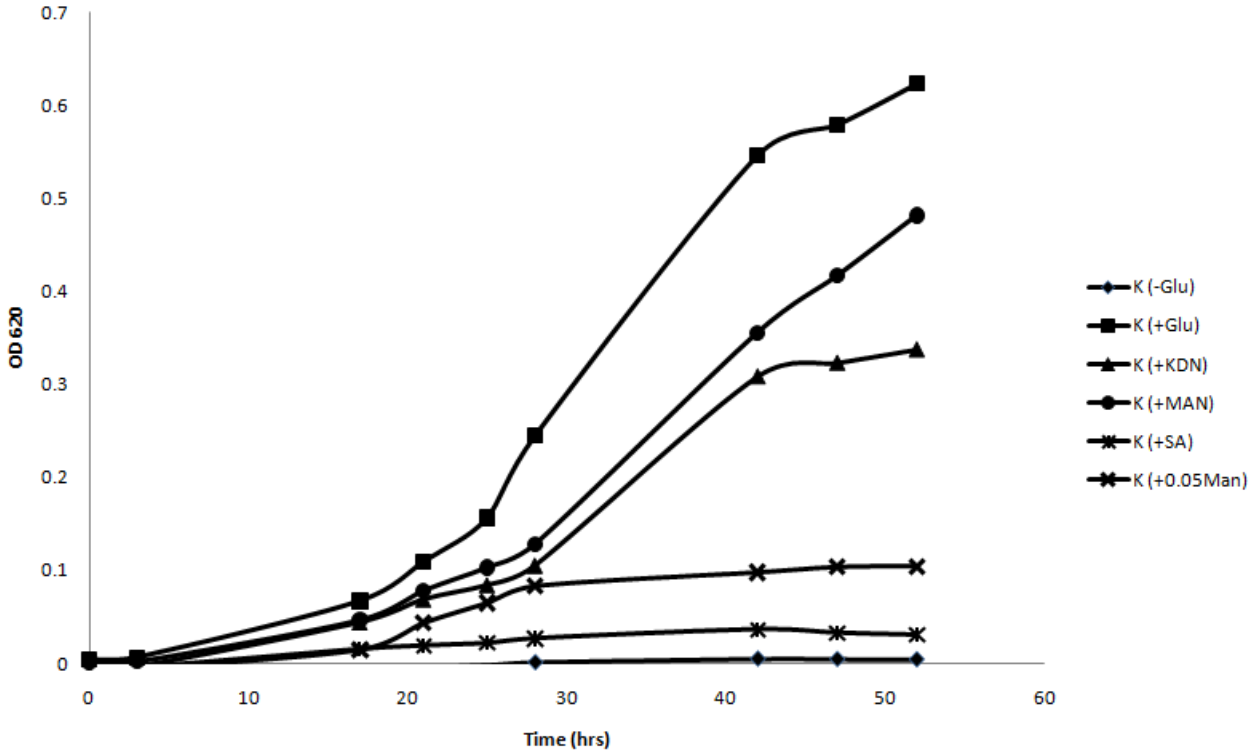
0.7
0.6
0.5
0.4
0.3
0.2
0.1
0
OD 620
0
10
20
30
40
50
60
Time (hrs)
K (-Glu)
K (+Glu)
K (+KDN)
K (+MAN)
K (+SA)
K (+0.05Man)